Three-Dimensional Neurite Characterization of Small Incision Lenticule Extraction Derived Lenticules

Francisco Bandeira,[1–3] Gary Hin-Fai Yam,[1,4,5] Yu-Chi Liu,[1,4,6] Kavya Devarajan,[1] and Jodhbir S. Mehta[1,4,6–8]

[1]Tissue Engineering and Stem Cell Group, Singapore Eye Research Institute, Singapore
[2]Federal University of São Paulo, Sao Paulo, Brazil
[3]São Gonçalo Eye Hospital, Rio de Janeiro, Brazil
[4]Eye-Academic Clinical Program, Duke-NUS Graduate Medical School, Singapore
[5]Experimental Microscopy Platform, Singapore Eye Research Institute, Singapore
[6]Singapore National Eye Centre, Singapore
[7]Department of Ophthalmology, Yong Loo Lin School of Medicine, National University of Singapore, Singapore
[8]School of Material Science and Engineering, Nanyang Technological University, Singapore

Correspondence: Jodhbir S. Mehta, Singapore Eye Research Institute, 20 College Road, The Academia, Discovery Tower Level 6, Singapore 169856, Singapore; jodmehta@gmail.com.

Submitted: May 26, 2019
Accepted: August 29, 2019

Citation: Bandeira F, Yam GH-F, Liu Y-C, Devarajan K, Mehta JS. Three-dimensional neurite characterization of small incision lenticule extraction derived lenticules. *Invest Ophthalmol Vis Sci*. 2019;60:4408–4415. https://doi.org/10.1167/iovs.19-27566

Purpose. We study the density and excitatory response of neurites, and Schwann cells (SCs) in fresh and cryopreserved stromal lenticules derived from small incision lenticule extraction (SMILE).

Methods. Human stromal lenticules ($n = 23$) were immunostained for β III-tubulin and imaged using spinning disk confocal laser microscopy, followed by three-dimensional reconstruction, to reveal neurite distribution. The lenticule neurite density (LND) was assessed using a validated neurite tracing and length measurement method with NeuronJ. LND was compared among groups of different lenticule thickness (71–165 μm) obtained from −3 to >−6 diopters (D) corrections. SCs were identified by marker expression and the laser effect on SC-neurite interaction was examined under transmission electron microscopy (TEM). Fresh porcine SMILE-lenticules ($n = 18$) were used for LND comparison among storage conditions and functional excitatory calcium response assay.

Results. Using a validated neurite length measurement method, we found an inverse correlation of LND with lenticule thickness. Higher LND was found in thinner lenticules obtained from lower power of correction ($r = -0.8925$, $P < 0.0001$), whereas total lenticule neurite lengths did not alter significantly with regards to lenticule thickness. SCs were identified by GAP43 and $p75^{NTR}$ expression and were closely associated with lenticule neurites under TEM. In porcine lenticules, LND and excitatory calcium response were reduced after cold and cryogenic storage, when compared to fresh lenticules.

Conclusions. The stromal neurites showed variations in density related to SMILE lenticule thickness and cryopreservation. With the presence of SC support and excitatory response, these neurite residues could retain minimal functionality that might serve as a potential advantage in the event of lenticule implantation.

Keywords: stromal lenticules, corneal nerves, corneal neurite function, refractive surgery, SMILE

Small incision lenticule extraction (SMILE) is a femtosecond laser (FSL) procedure that has become an alternative to Laser in situ keratomileusis (LASIK) for the treatment of myopia and myopic astigmatism.[1] During SMILE, after femtosecond laser photodisruption, a stromal lenticule is dissected and manually extracted.[2] Since the cornea is the most innervated tissue in the human body,[3] the immediate side effect after SMILE is corneal denervation.[4] Similarly for LASIK, following flap creation and stromal ablation, there is a depth-dependent denervation.[5,6] Hence, the depth of the cap and thickness of extracted lenticule should influence the degree of denervation after SMILE.

Nerve transection in refractive surgery causes an inflammatory reaction[7] and secretion of growth factors and neurotrophins by activated stromal keratocytes, stromal fibroblasts, and corneal epithelium.[8,9] Denervation activates regeneration-associated genes, that will promote axonal growth with functional axoplasmic calcium signaling.[9,10] The presence of Schwann cells (SCs) is critical in mediating nerve survival and extension of the newly formed nerve fibrils inside the corneal stroma.[11,12] Incomplete nerve regeneration after corneal surgery disrupts the ocular surface homeostasis by reducing tear reflex, impairing epithelial healing, and decreasing corneal sensitivity.[13]

Nerve regeneration following SMILE is different from LASIK.[14] Patients who have undergone LASIK experience a pronounced denervation[5] due to extensive stromal cell death from excimer laser ablation[15] and flap creation; hence, the nerve regeneration is delayed.[16] In contrast, SMILE results in less reduction in subbasal nerve density, faster stromal wound

Table 1. Antibodies Used in This Study

	Antibody	Source	Working Concentration
1	βIII-tubulin	Covance MMS435P	0.5 μg/mL
2	GAP43	Novus NB300-143	0.5 μg/mL
3	$P75^{NTR}$	Millipore AB1554	0.5 μg/mL
4	Phalloidin-AlexaFluor 594 conjugate	Invitrogen	0.5 μg/mL
5	AlexaFluor 488 goat anti-mouse/rabbit IgG (H+L)	Jackson ImmunoRes Lab	Immunostaining: 1:700
6	RedX-conjugated goat anti-mouse/rabbit IgG (H+L)	Jackson ImmunoRes Lab	Immunostaining: 1:700

healing,[17] and corneal sensation recovery.[18] However, the subbasal nerve density does not return to baseline values even by 6 months after SMILE.[14] In patients who have undergone LASIK, restoring the subbasal nerve density takes even longer. In vivo confocal microscopy (IVCM) detected abnormal reinnervation features with nerve density lower than baseline even 5 years after LASIK.[19]

The distribution of neurites inside the cornea is heterogeneous, with most of the axons located in the anterior stroma.[20] Following SMILE, the anterior FSL planar cut typically is made at a depth of 110 to 160 μm from the epithelial surface,[21,22] the posterior resection plane may extend to 300 μm depth depending on the power of correction.[23] The relationship between the thickness of resected lenticules (i.e., the amount of refractive correction), and the degree of denervation after SMILE is unclear. Nevertheless, it currently is possible to measure the total lenticule neurite density (LND) using superresolution ultrawide field confocal laser microscopy combined with three-dimensional (3D) z-stack reconstruction.[4] Thus, neurite tracing and length measurement will allude to lenticule neurite density, which can be used as a surrogate marker to assess the degree of denervation with respect to lenticule thickness.

Several ongoing studies are investigating the clinical applications of SMILE-derived lenticules, which would otherwise be discarded.[24–28] Lenticule implantation has been shown to be efficacious in animals[25,28] and humans.[24,25,29,30] It causes a low rate of haze formation, minimal inflammatory reaction, and maintenance of corneal transparency.[30,31] Preoperatively, lenticules may need to be transported, stored, and tailored to the appropriate thickness and shape according to specific indications (e.g., hyperopia, presbyopia, or stromal volume expansion).[21,30,32,33] Recently, the feasibility and safety of cryostorage of SMILE lenticules has been described.[25,31,34,35] However, the influence of cryostorage on neurite density, viability, as well as neurite-glial cell interaction is unknown.

We first validated a method to measure neurite length, allowing the quantification of neurite density in SMILE lenticules. Various factors affecting LND, such as the power of correction (lenticule volume) and storage conditions, were evaluated. The SC support to neurites inside lenticules and the excitatory Ca^{++} response also were characterized.

Materials and Methods

Corneal Lenticules

The study was approved by the institutional review board of SingHealth, Singapore (CIRB/109/A) and conducted in accordance with the Declaration of Helsinki. Informed consent was obtained from all patients. A total of 23 human lenticules were obtained from patients who underwent SMILE at the Singapore National Eye Centre, Singapore (Supplementary Fig. S1A). SMILE was performed by a single surgeon (JM) using a 500 kHz FSL-assisted VisuMax (Carl Zeiss Meditec, Jena, Germany).[32] Human lenticules were submerged immediately in PBS (0.1 M, pH 7.5; Life Technologies, Carlsbad, CA, USA), transferred to the laboratory within 30 minutes on ice, and fixed in paraformaldehyde for immunostaining. The method of neurite length measurement was optimized with three lenticules (random thickness). Another 12 lenticules were placed into groups with thickness according to the power of correction in terms of diopter (D). Group 1, <−3 D ($n = 4$ lenticules); group 2, from −3 to −6 D ($n = 4$); and group 3, >−6 D ($n = 4$). The remaining eight human lenticules were used for transmission electron microscopy (TEM; $n = 4$) and immunohistochemistry ($n = 4$) (Supplementary Fig. S1B).

In addition, fresh porcine lenticules ($n = 18$) were recruited for assessing neurite changes under different storage conditions ($n = 12$) and excitatory calcium response ($n = 6$). Porcine eyes were enucleated within 6 hours after death and the SMILE procedure was performed similarly as above.[32] In brief, the corneal curvature was set to 7.8 mm and lenticule diameter was 6.5 mm. According to the Visumax software, a −3D correction power generated a biconvex lenticule with a minimum thickness of 30 μm at the peripheral edge and maximum thickness of 65 μm at the center. The 7.3-mm (diameter) cap was cut with a 2.55-mm incision positioned at 135°, with a cap thickness of 110 μm. After laser application, the stromal lenticule was freed by using a blunt spatula (AE 4226; Asico, Westmont, IL, USA), extracted through the incision. The transportation procedure and fixation of the samples followed exactly the same steps as stated above for human lenticules.

Immunostaining

Lenticules were fixed with freshly prepared neutral-buffered 4% paraformaldehyde (PFA; Sigma-Aldrich Corp., St. Louis, MO, USA) for 10 minutes at room temperature, washed with PBS, and quenched with ice-cold 50 mM ammonium chloride (Sigma-Aldrich Corp.) for 5 minutes on ice.[36] After permeabilization and blocking with 0.15% saponin (Sigma-Aldrich Corp.), 2% bovine BSA and 5% normal goat serum (Invitrogen, Carlsbad, CA, USA), samples were incubated with primary antibodies (Table 1) for an hour at room temperature. After washes, the signal was revealed by appropriate fluorescence-conjugated secondary antibody. Samples were then washed, mounted in FluorShield containing 4′,6-diamidino-2-phenylindole (DAPI; Santa Cruz Biotechnology, Inc., Dallas, TX, USA), and examined under confocal microscopy (CSU W1 Spinning Disk; Nikon; Tokyo, Japan), respectively.

Spinning Disk Microscopy and Image Reconstruction

The lenticules were scanned with a confocal laser spinning disk microscope (CSU W1 Spinning Disk; Nikon) using the "scan large image" protocol (NIS Elements, v. 4.40.00). Under ×10 objective, the scan boundary was marked with an extra 20 μm beyond the outer sample margin to account for the nonparallel distension of the planoconvex lenticule when

placed as flat-mount. The pixel size was 0.64 × 0.64 μm, and serial z-stacks at 5 μm depth. Mosaic images were acquired and automatically stitched with XY overlap set at 15%. Under a maximum intensity projection function, all z-stacks were merged into a single two-dimensional (2D) image for neurite length analysis.

Neurite Tracing and LND Calculation

Neuron-specific βIII-tubulin (TuJ1)–stained neurites were traced using NeuronJ plugin under ImageJ/Fiji (version 2.0.0-rc-68/1.52e, available in the public domain at http://imageJ.net).[37] The neurite length in pixels was converted to micrometers according to the scale bar provided on confocal images and "total neurite length" (TNL) was calculated. The volume of lenticules was determined using an established formula calculating the ablation volume in excimer laser surgery: $VM \approx D(S/9)^4$, in which D is the intended dioptric correction and S is the lenticule diameter.[38] The lenticule neurite density (LND) then was calculated by dividing TNL by the respective lenticule volume.

Validation of Neurite Length Measurement Method

Two independent, masked observers (FB and YL) performed the same procedure of neurite tracing and length measurement using a cohort of 15 lenticules. The exercise was repeated after 1 week. The intraobserver repeatability and interobserver reproducibility were assessed by Bland-Altman analysis.

Porcine Lenticule Storage

The freshly extracted porcine lenticules were washed in PBS twice and randomly allocated to three groups: Group 1, no storage ($n = 4$ lenticules; the lenticules were immediately fixed in PFA for 10 minutes); Group 2, cold storage in PBS at 4°C for 48 hours ($n = 4$); and Group 3, cold storage in PBS at 4°C for 48 hours, followed by frozen storage in a cryoprotective medium (Dulbecco's modified Eagle medium [DMEM]; Invitrogen) with 10% (vol/vol) fetal bovine serum (FBS; Gibco Laboratories, Gaithersburg, MD, USA) under liquid nitrogen for 1 month ($n = 4$). After cold and frozen storages, lenticules were washed with PBS thrice and fixed in paraformaldehyde (PFA) for 10 minutes. All samples were immunostained for TuJ1; and TNL and LND were compared.

Excitatory Calcium Response Assay

Porcine lenticules were marked for orientation by a small irregular notch before experiment. They were processed: (1) after 4° cold storage for 48 hours ($n = 3$) and (2) after frozen storage under liquid nitrogen for a month ($n = 3$), washed with $Ca^{2+}Mg^{2+}$-free Hank's balanced salt solution (HBSS, Invitrogen) five times to remove free divalent ions. They were incubated in fluo-4-acetoxymethyl (Fluo-4AM) ester (5 μM, Invitrogen) and 0.1% pluronic F-127 (Sigma-Aldrich Corp.) in HBSS for 30 minutes in dark. Immediately after the addition of 1 μM glutamate (final concentration), the lenticules were examined under wide-field confocal microscopy (CSU W1). The lenticules then were fixed and processed for TuJ1 immunostaining as described earlier and imaged again by confocal microscopy. Montaged images of Ca^{2+} response and TuJ1 staining were precisely overlaid according to the marked orientation using Photoshop software (version mL; Adobe, San Jose, CA, USA). Colocalized signals of Ca^{2+} and TuJ1 were traced by NeuronJ and the portion with Ca^{2+} signal along the Tuj1-stained neurite was determined.

Statistics

The Bland-Altman plot was used to determine intra- and interobserver agreements on neurite length measurement. The reproducibility values were calculated as mean bias and 95% limits of agreement (LoA). Wilcoxon matched-pairs signed rank test was used for the differences within intra- and interobserver measurements. Differences between LND in human lenticule groups were assessed with the Kruskal-Wallis 2-way analysis, while differences in porcine LND between time-points in storage study were analyzed with Friedman's test. Correlations between preoperative corneal characteristics, lenticule design variables, and LND were performed with Pearson's correlation test. All values were described as mean ± SD, unless stated otherwise. Prism 6.0 (GraphPad Software, La Jolla, CA, USA) was used to generate graphs and statistical analysis. $P < 0.05$ was considered statistically significant.

Results

SMILE Lenticule Neurite Distribution and Morphology

Wide-field confocal scanning and 3D reconstruction captured high-resolution neurite profile (Fig. 1A) within stromal lenticules, for neurite tracing and linear length determination (Figs. 1B, 1C). TuJ1-stained neurites appeared as short segments with infrequent branches inside the stromal lenticules (Figs. 1D, 1E). The thicker neurites tended to follow a straight path, whereas thin fibers had more beading and tortuosity (Fig. 1F, arrows). A representative video of the 3D neurite distribution inside the lenticules is shown in Supplementary video S1.

Method Validation of Neurite Length Measurement

Two independent observers performed neurite tracing and length measurement on montaged images of 15 lenticules, using NeuronJ. In each sample, the lengths of 80 to 130 neurites were measured. There was no significant intraobserver difference. The intraobserver mean bias was –0.74 ± 4.45 mm for observer A and –0.71 ± 5.21 mm for observer B. LoA ranged from –9.46 to 7.99 and –9.50 to 10.92 mm, respectively. Good interobserver agreement was also achieved as shown by the insignificant mean biases and LoA for different parameters. The coefficient of repeatability was 17.04 and 17.83 for interobserver measurements at first and second time points, respectively.

TNL and LND for Different Lenticule Thickness

The demographic information of patients and details of the surgical plan are depicted in Table 2, and representative images of SMILE-lenticules are shown in Figures 2A to 2C. The mean power of correction was –2.28 ± 0.21 D for Group 1 (<–3 D), –5.31 ± 1.05 D for Group 2 (–3 to –6 D), and –9.69 ± 0.88 D for Group 3 (>–6 D). There was no significant difference concerning TNL among groups ($P = 0.63$, Friedman test, Fig. 2D). The neurite widths and lengths ranged from 5 to 20 μm and 0.1 to 3.55 mm, respectively ($n = 1360$ neurites). Mean lenticule volume was significantly different among groups ($P < 0.05$, Friedman test) and mean LND was also significantly higher in Group 1 compared to Groups 2 and 3 ($P < 0.05$, Friedman test, Fig. 2E). Mean LND was 63.41 ± 11.17, 37.45 ± 20.14, and 22.41 ± 4.59 mm/mm^3 for Groups 1 to 3, respectively. The LND showed significant inverse correlation with the power of correction ($r = –0.8925$, $P < 0.0001$, Fig. 3A). There was a trend of increasing LND in thinner lenticules

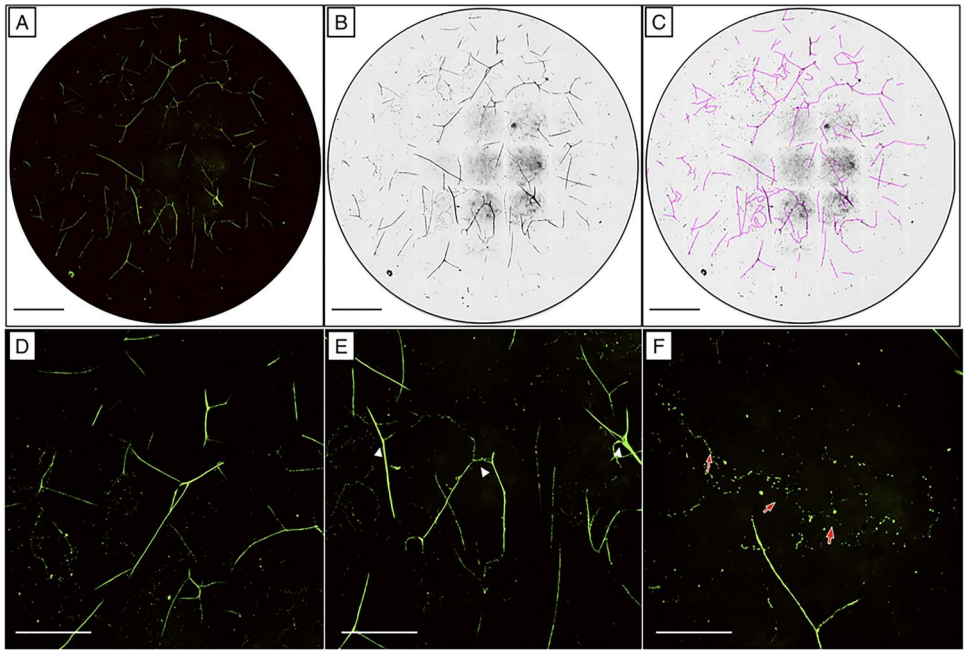

Figure 1. Representative reconstructed images of TuJ1-stained neurites for tracing and length measurement using NeuronJ plugin in ImageJ/Fiji software. (**A**) The 2D maximum intensity projection image reconstructed from z-serial images using wide-field spinning disk confocal laser microscopy. (**B**) Conversion to 8-bit gray-scale image. (**C**) Tracing of TuJ1-stained neurites with NeuronJ plugin. (**D–F**) High magnification images of representative neurites. (**D**) Distribution of neurite segments inside the lenticule. (**E**) Neurite branching, bifurcation, and interconnections. (**F**) Thin sinuous neurite fibers with beadings (*red arrows*). *Scale bars*: 1 mm (**A–C**); 500 μm (**D–F**).

(Fig. 3B). Other parameters, including patient age, preoperative central corneal thickness (CCT), keratometric readings, cap thickness, and lenticule diameters, were not significantly correlated with LND.

Ultrastructural Morphology of Stromal Neurites and Glial Support

Under TEM (Materials and Methods in Supplementary Information), the neurite fibrils were nonmyelinated. They were running in parallel to and across the collagen lamellae (Supplementary Fig. S1A) and occasionally in contact with stromal cells. At higher magnification, the axons were composed of numerous neurofilaments, neurotubuli, and mitochondria with electron-lucent cristae (Supplementary Fig. S1B). Some of these structures were located within the cytoplasmic invagination of nucleated cells, the SCs. The SC nucleus was prominent with condensed chromatin, whereas the loose cytoplasm contained numerous intercellular spaces that formed thin pockets wrapping around the axons (Supplementary Fig. S1C). By immunofluorescence, the SC cytoplasm was positive to growth associated protein 43 (GAP43) staining and enclosed several bundles of neurofilaments stained by TuJ1 (Figs. 4A–C). The staining of $p75^{NTR}$ was mostly located along SC basal lamina surrounding the axons (Figs. 4D–F).

Effect of Lenticule Storage on LND

Fresh porcine lenticules ($n = 4$) presented a mean LND of 55.02 ± 4.34 mm/mm^3. The LND was significantly reduced after cold or frozen storage ($P < 0.01$). LND was 32.01 ± 5.77 mm/mm^3 after 4°C storage for 48 hours and reduced to 20.28 ± 5.11 mm/mm^3 after additional storage under liquid N_2 for a month (Fig. 5). There was no significant difference of LND between the storage groups.

Excitatory Calcium Response of Lenticule Neurites

Excitatory neurotransmitter-induced calcium changes were detected along porcine lenticule neurites. Immediately after the addition of glutamate, the lenticule neurites showed

Table 2. Patient Demographics Information

	Group 1 (> −3 D)	Group 2 (−3 D to −6D)	Group 3 (< −6 D)	*P*
Age (years)	34.50 ± 6.35 (29–40)	33.00 ± 4.69 (30–40)	30.50 ± 0.58 (30–31)	0.77
Power (D)	−2.28 ± 0.21 (−2 to −2.5)	−5.31 ± 1.05 (−3 to −6)	−9.69 ± 0.88 (−8 to −10.5)	<0.001
Pachymetry (μm)	546.50 ± 11.47 (536–562)	549.00 ± 14.97 (533–569)	565.50 ± 10.41 (550–572)	0.06
Km (D)	45.08 ± 0.09 (44.95–45.15)	42.71 ± 0.69 (42–43.3)	43.99 ± 0.65 (43.20–44.5)	<0.005
Diameter (mm)	6.75 ± 0.06 (6.7–6.8)	6.50 ± 0.00	6.23 ± 0.05 (6.3–6.4)	<0.001
Volume (mm^3)	0.72 ± 0.08 (0.61–0.81)	1.44 ± 0.28 (1.02–1.63)	2.36 ± 0.24 (2.01–2.56)	<0.001
Cap thickness (μm)	125 ± 5.77 (120–130)	120 ± 0.00	120 ± 0.00	0.27
TNL (mm)	45.66 ± 8.49 (36–56)	50.20 ± 13.93 (36–68)	52.46 ± 8.99 (41–63)	0.67
LND (mm/mm^3)	63.41 ± 11.17 (50.44–77.21)	37.45 ± 20.14 (22.65–67.08)	22.41 ± 4.59 (16.15–26)	<0.05
Preservation time (days)	512.75 ± 41.91 (474–549)	443.75 ± 61.27 (369–519)	436.00 ± 106.20 (344–548)	0.24

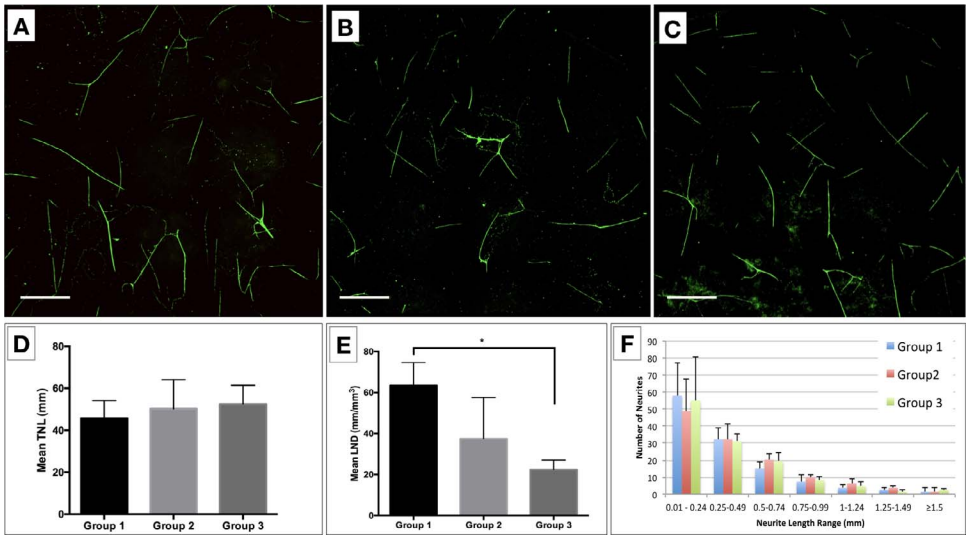

Figure 2. Comparison of neurite lengths and densities among groups of different lenticule thickness. (**A–C**). Representative reconstructed images of TuJ1-stained neurites in (**A**) Group 1 (<–3 D); (**B**) Group 2 (–3 to –6 D) and (**C**) Group 3 (>–6 D). (**D**) No significant difference of mean TNL among groups ($P > 0.05$, 1-way ANOVA on ranks). (**E**) Comparison of mean LND among groups. *Statistical significant difference was shown between Groups 1 and 3 ($P < 0.05$). (**F**) A frequency plot of neurite length distribution in different groups. Short neurites (<0.25 mm) were predominantly present inside lenticules. *Scale bars*: 500 μm (**A–C**).

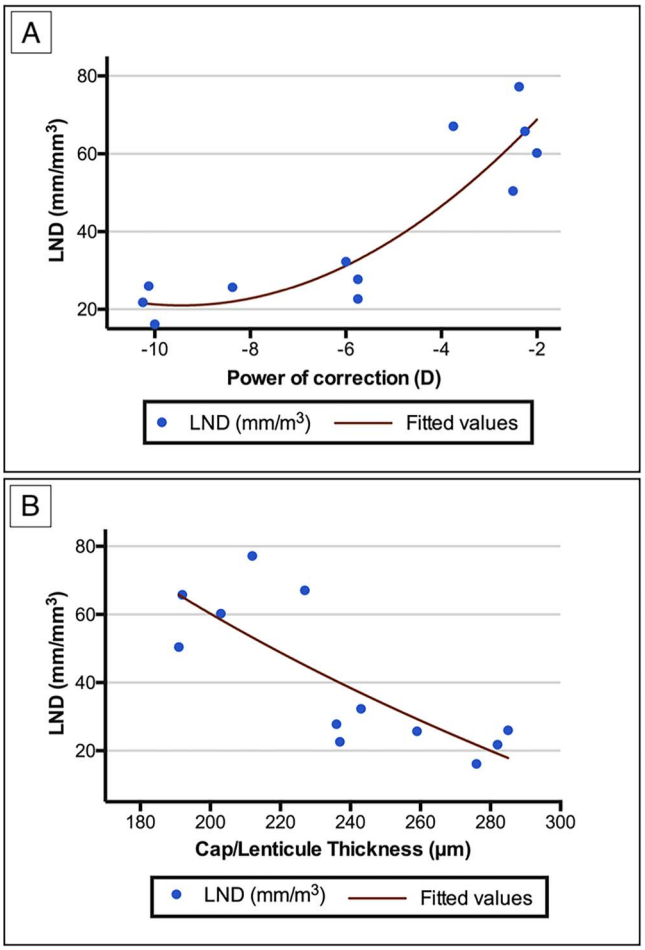

Figure 3. Correlations between LND and surgical parameters. (**A**) Quadratic prediction plot of LND with power of correction in terms of diopter D. (**B**) Quadratic prediction plot of LND with lenticule depth (sum of cap and lenticule thickness). In SMILE procedures, the cap thickness was set at 120 μm.

calcium level changes by displaying positive Fluo-4-AM signals along thin linear elongated structures (Figs. 6A–F). Using NeuronJ tracing and length measurement, after 48 hours at 4° cold storage, the porcine lenticules had 35.6% ± 9.8% of TuJ1-neurites having fluo-4-AM signal changes. For the frozen-stored lenticules, the Fluo-4-AM/TuJ1 colocalized signal was markedly reduced and the percentage was 6.6% ± 2.8% (Figs. 6G–L).

Discussion

The neurite profile in SMILE-lenticules was characterized by TuJ1 immunofluorescence, followed by wide-field confocal microscopy combined with 3D reconstruction. We first validated a method of neurite tracing and length measurement with NeuronJ and subsequently used this validated method to determine the LND. The LND in lenticules with thickness >–6 D was significantly less than that in <–3 D lenticules, whereas LND also was significantly reduced in lenticules that had undergone cold or frozen storage when compared to fresh lenticules. Ultrastructural examination illustrated a close Schwann cell-neurite interaction. Functional excitatory re-

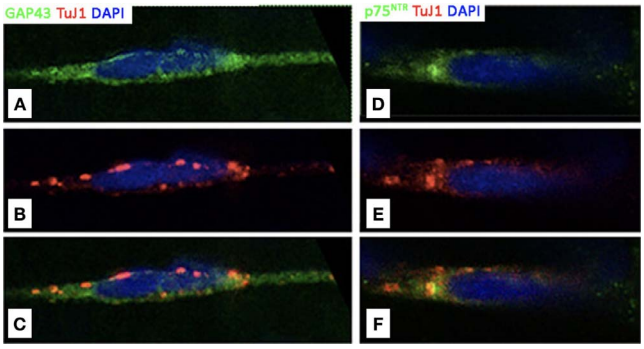

Figure 4. Interaction between lenticule neurites and SCs. Colocalization of SC marker expression and stromal neurites by confocal immunofluorescence: (**A–C**) GAP43 (*green*) and TuJ1 (*red*). (**D–F**) $p75^{NTR}$ (*green*) and TuJ1 (*red*).

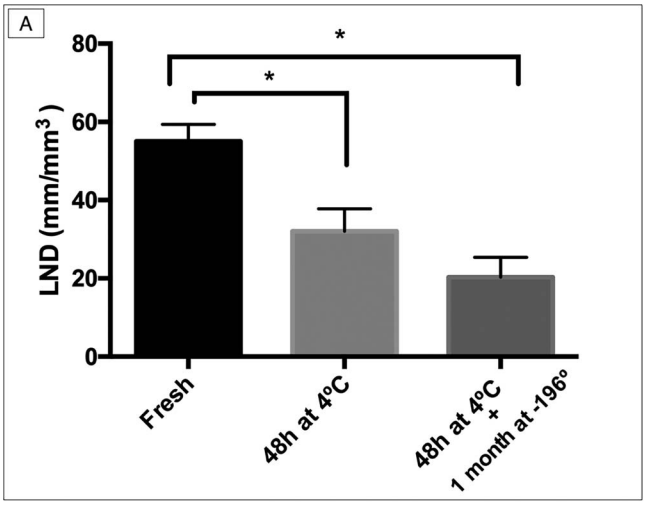

B	Fresh	48h at 4ºC	48hº at 4ºC + 1 month at -196ºC	p
LND (mm/mm³)	55.02±4.34 (50.33 to 60.71)	32.01±5.77 (26.07 to 39.49)	20.28±5.11 (16.33 to 27.33)	<0.01

FIGURE 5. Comparison of LNDs in porcine lenticules after different storage conditions. (**A**) Comparison of mean LNDs between fresh collection, 4°C storage for 48 hours and 4°C storage for 48 hours followed by −196°C cryostorage (under liquid N_2) for 1 month (*$P <$ 0.01; Friedman test). (**B**) LND values in mean ± SD (range) for each group.

sponse of remaining neurites was demonstrated by neurotransmitter-mediated Ca^{++} signaling, which was reduced following cryostorage.

The effect of SMILE on corneal nerve density has been investigated using IVCM.[18,39] However, it has not been possible to correlate denervation with the power of correction. This could be due to the inherent limitation of ICVM, which has a small region of interest (<500 μm²), and the lack of standard methodology for nerve density analysis.[40] The study of LND could indicate the denervation effect after SMILE. We previously described the effect of SMILE on corneal reinnervation using a rabbit model, but the lenticule neurite profiles were analyzed on 2D sections with immunostaining.[4] Here, we have devised a 3D reconstructed neurite profile and quantification strategy, accounting for the lenticule volume.[38] Using super-resolution wide-field spinning disk confocal laser microscopy to serially capture z-stacks for the entire volume of the lenticule (6.2–6.8 mm diameter), we were able to create a montaged 2D picture for the entire lenticule through software-based auto-stitching with XY overlap set at 15%. This offered an opportunity to analyze intralenticular structures at different depths for objective tracing and quantification.

We performed a validation process to evaluate the reproducibility and repeatability of neurite tracing and length measurement by two independent observers. Our results showed that this assay was a highly reproducible tool for quantitative measurement of lenticule neurite length. The mean difference between measurements by the same observer was small along the entire range of refractive corrections (−2.50 to −10.50 D, $P < 0.05$). The interobserver means of difference were also small. Inter- and intraobserver LoA variations were low.

The neurite density changes in different lenticular volumes could act as a surrogate marker for denervation after SMILE. Most reports on SMILE-induced denervation have documented the clinical consequences of nerve transection postoperatively,[41] instead of directly assessing the extent of lenticule denervation. Our results indicated that LND changes were not directly associated with the volume of lenticule resection. Instead, there was an inverse exponential correlation between them. The resection of thin lenticules (low power of correction) was mostly performed in the anterior stromal region, where the majority of stromal nerves are located,[20] which could explain the greater LND found in thinner lenticules. In correlating the preoperative demographics and LND, approximately 50% of neurites were located in the region between 180 and 240 μm below the epithelium. In this study, the lenticule volume was calculated based on Munnerlyn's formula for LASIK,[38] whereas the exact calculation for SMILE lenticule is a proprietary information.[42] Nevertheless, other studies have shown that the corneal volume removed after lenticule extraction was approximate to that obtained with Munnerlyn's formula,[43] and this supports the data found here.

The study of LND is important because the remaining axon scaffolds in the lenticule may influence post-implantation nerve regeneration. We studied the relationship between neurite-associated microtubules and the supporting SCs. The

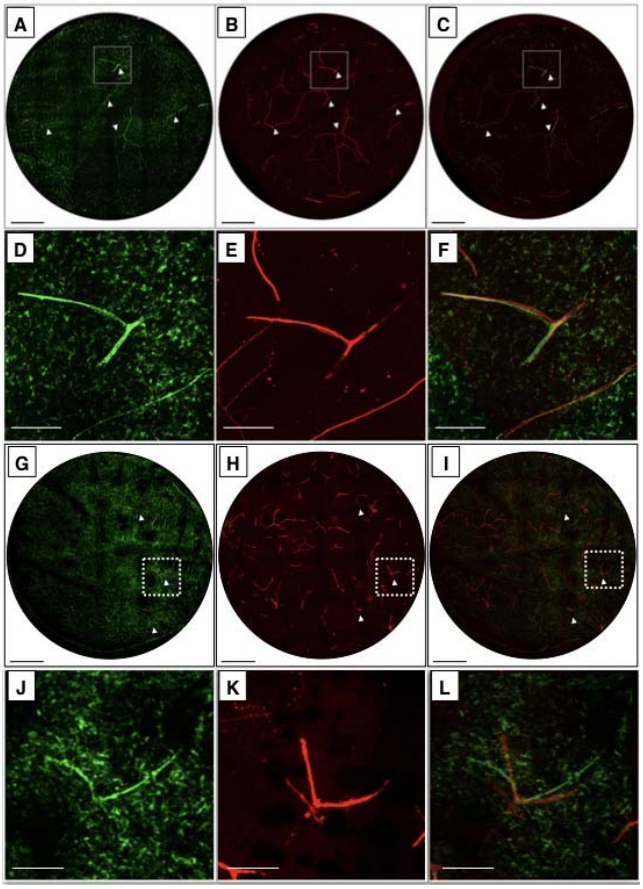

FIGURE 6. Excitatory calcium response by porcine lenticule neurites. (**A–F**) Fresh lenticules. (**A**, **D**) Fluo-4AM signals after glutamate stimulation. (**B**, **E**) TuJ1 staining of neurites. (**C**, **F**) Overlay of Fluo-4AM and TuJ1 signals. The *marked region* in the wide-field confocal image of (**A–C**) denoted the region of (**D–F**). (**G–L**) Lenticules after cryostorage at −196°C for a month. (**G**, **J**) Fluo-4AM signals after glutamate stimulation. (**H**, **K**) TuJ1 staining of neurites. (**I**, **L**) Overlay of Fluo-4AM and TuJ1 signals. The marked region in the wide-field confocal image of (**G–I**) denoted the region of **J–L**. *White arrowheads* indicate the neurite fragment with colocalized Fluo-4AM and TuJ1 signals. *Scale bars*: 1 mm (**A–C**, **G–I**); 500 μm (**D–F**, **J–L**).

presence of SCs inside the lenticules was distinguished by SC marker expression, including GAP43 and $p75^{NTR}$. These signals were colocalized with TuJ1-stained neurites. The SC support is known to be essential for the maintenance of neurite function upon stimulation.[41] They provide topographic cues that are associated with neurite growth.[41] In addition, SCs have been shown to proliferate and serve as tracks for axonal regrowth. Thus, their presence in the lenticule stroma indicates a potential for guided reinnervation after lenticule reimplantation.[42] Nevertheless, the underlying mechanism of neurite growth and the role of SC requires further investigations.

We also evaluated the effect of lenticule storage on LND changes. In nerve grafts, mid to long term cryostorage (for 2–4 weeks) reduced immunogenicity, while maintaining SC viability.[43] Previous lenticule storage studies have shown that different cryoprotective media, such as glycerol and dimethylsulfoxide (DMSO), had negligible effects on lenticule transparency and collagen fibril pattern.[34] However, our results have shown that the neurite profile was affected by lenticule preservation. We chose cold storage at 4°C for 48 hours to simulate the cold transportation of lenticules from surgery to tissue processing and cryogenic storage facility.[34] The lenticules then were cryostored under liquid N_2 for a month. We noticed that LND was significantly reduced following both stages. Hence, this indicated that most of the nerve degeneration occurred during the cold transportation of lenticules.

The neurite function was assessed using an excitatory Ca^{++} response assay, in which the cellular Ca^{++} signal changed as a response to a neurostimulant. We showed that Ca^{++} signals were distributed along the neurites with partial colocalization with Tuj1 staining. Upon stimulation with glutamate, positive Ca^{++} signal was detected in treated lenticules, but not for lenticules treated with PBS or sham control without glutamate. This indicated the potential functional response of remaining neurites in the lenticules. However, we were unable to quantify such excitatory response because this occurred in milliseconds after stimulation. The serial z-stack for whole neurite capture requires a long scanning time and this would have surpassed the rapid Ca^{++} responses. Using porcine lenticules, a marked reduction of Ca^{++} response was observed following frozen storage. This could be attributed to the hypothermic effects, during freezing and thawing, that can affect nerve fiber viability, leading to cessation of intracellular calcium movement.[44] Further investigation on cryostorage conditions (including type of cryopreservative media, freeze and thaw duration, and stepwise temperature changes) may provide information on preserving neurite activity.

The rationale of investigating the LND changes upon lenticule preservation resided in the hypothesis that the residual neurites and their glial support could affect the posttransplantation nerve regeneration. Customized lenticule reimplantation after storage is an emerging clinical treatment for hyperopia, presbyopia and ectatic disorders.[24–31,33–34] Nerve regeneration is highly dependent on the stromal matrix environment (such as tracks of neurite residues and glial interactions). Hence, our study characterized the neurite distribution and density changes within the lenticules as well as the residual excitatory response, in association with cryopreservation. Cryopreservation is required to make the logistics of surgical planning and finding a suitable donor lenticule feasible. These data showed that even after storage, the lenticule neurite residues could retain minimal functionality, which could have potential advantage in reinnervation after lenticule implantation.

Even though it is tempting to suggest the presence of SCs will be beneficial to reinnervation, we have to take into consideration previous reports of reinnervation following keratoplasty. Studies have shown limited stromal reinnervation in donor corneas procured in cold storage medium.[45,46] Hence, the effect of storage medium on reinnervation is largely unknown, and requires further investigation. Another consideration is that preservation following lenticule extraction can be performed immediately as opposed to corneal tissue. Donor corneas from eye banks are subject to postmortem deterioration between 0 and 6 hours at room temperature or 0 and 24 hours of refrigeration, which might also affect SC viability. In addition, the surgical techniques for lenticule implantation and keratoplasty are markedly different concerning incision size and denervation; hence, the minimal invasive lenticule implantation may favor better nerve recovery.

In summary, we characterized the neurite distribution in SMILE-derived lenticules. This has brought a greater understanding regarding the effect of refractive correction and denervation following SMILE. The presence of potentially functional neurite residues, SCs, and the glial microenvironment may affect the reinnervation after SMILE lenticule implantation. Our study was limited by its descriptive nature; hence, it is beyond the scope of this study to propose an in depth discussion on the poorly understood mechanism behind postoperative corneal reinnervation. Future studies in animals should be conducted focusing on whether regrowth of stromal nerves inside lenticules can occur, and if this will influence postoperative nerve densities.

Acknowledgments

The authors thank Hla Myint Htoon (Statistics Platform, Singapore Eye Research Institute) for discussion on statistical analysis, SingHealth Advanced Bioimaging Core Facilities for wide-field spinning disk confocal microscopy, and Experimental Microscopy Platform, Singapore Eye Research Institute for transmission electron microscopy.

Disclosure: **F. Bandeira**, None; **G.H.-F. Yam**, None; **Y.-C. Liu**, None; **K. Devarajan**, None; **J.S. Mehta**, None

References

1. Doane JF, Cauble JE, Rickstrew JJ, Tuckfield JQ. Small incision lenticule extraction SMILE – the future of refractive surgery is here. *Mo Med*. 2018;115:82–84.
2. Liu YC, Riau AK, JS M. Small incision lenticule extraction (SMILE). In: Krachmer JH, Mannis MJ, Holland EJ, eds. *Cornea*. 4th ed. Philadelphia: Elsevier; 2016.
3. Marfurt CF, Cox J, Deek S, Dvorscak L. Anatomy of the human corneal innervation. *Exp Eye Res*. 2010;90:478–492.
4. Mohamed-Noriega K, Riau AK, Lwin NC, Chaurasia SS, Tan DT, Mehta JS. Early corneal nerve damage and recovery following small incision lenticule extraction (SMILE) and laser in situ keratomileusis (LASIK). *Invest Ophthalmol Vis Sci*. 2014;55:1823–1834.
5. Nassaralla BA, McLeod SD, Boteon JE, Nassaralla JJ Jr. The effect of hinge position and depth plate on the rate of recovery of corneal sensation following LASIK. *Am J Ophthalmol*. 2005;139:118–124.
6. Nassaralla BA, McLeod SD, Nassaralla JoJ. Effect of myopic LASIK on human corneal sensitivity. *Ophthalmology*. 2003; 110:497–502.
7. Li Z, Burns AR, Han L, Rumbaut RE, Smith CW. IL-17 and VEGF are necessary for efficient corneal nerve regeneration. *Am J Pathol*. 2011;178:1106–1116.
8. Gao S, Li S, Liu L, et al. Early changes in ocular surface and tear inflammatory mediators after small-incision lenticule extraction and femtosecond laser-assisted laser in situ keratomileusis. *PLoS One*. 2014;9:e107370.

9. Chaudhary S, Namavari A, Yco L, et al. Neurotrophins and nerve regeneration-associated genes are expressed in the cornea after lamellar flap surgery. *Cornea*. 2012;31:1460–1467.
10. Pham TL, He J, Kakazu AH, Jun B, Bazan NG, Bazan HEP. Defining a mechanistic link between pigment epithelium-derived factor, docosahexaenoic acid, and corneal nerve regeneration. *J Biol Chem*. 2017;292:18486–18499.
11. Conrad AH, Albrecht M, Pettit-Scott M, Conrad GW. Embryonic corneal Schwann cells express some Schwann cell marker mRNAs, but no mature Schwann Cell marker proteins. *Invest Ophthalmol Vis Sci*. 2009;50:4173–4184.
12. Linna TU, Perez-Santonja JJ, Tervo KM, Sakla HF, Alio y Sanz JL, Tervo TM. Recovery of corneal nerve morphology following laser in situ keratomileusis. *Exp Eye Res*. 1998;66:755–763.
13. Müller LJ, Marfurt CF, Kruse F, Tervo TMT. Corneal nerves: structure, contents and function. *Exp Eye Res*. 2003;76:521–542.
14. Bandeira F, Yusoff NZ, Yam GH, Mehta JS. Corneal re-innervation following refractive surgery treatments. *Neurol Regen Res*. 2019;14:557–565.
15. Wilson SE. Analysis of the keratocyte apoptosis, keratocyte proliferation, and myofibroblast transformation responses after photorefractive keratectomy and laser in situ keratomileusis. *Trans Am Ophthalmol Soc*. 2002;100:411–433.
16. Erie JC, McLaren JW, Hodge DO, Bourne WM. Recovery of corneal subbasal nerve density after PRK and LASIK. *Am J Ophthalmol*. 2005;140:1059–1064.
17. de Medeiros FW, Kaur H, Agrawal V, et al. Effect of femtosecond laser energy level on corneal stromal cell death and inflammation. *J Refract Surg*. 2009;25:869–874.
18. Agca A, Cankaya KI, Yilmaz I, et al. Fellow eye comparison of nerve fiber regeneration after SMILE and femtosecond laser-assisted LASIK: a confocal microscopy study. *J Refract Surg*. 2015;31:594–598.
19. Li M, Niu L, Qin B, et al. Confocal comparison of corneal reinnervation after small incision lenticule extraction (SMILE) and femtosecond laser in situ keratomileusis (FS-LASIK). *PLoS One*. 2013;8 (:e81435.
20. Oliveira-Soto L, Efron N. Morphology of corneal nerves using confocal microscopy. *Cornea*. 2001;20:374–384.
21. Damgaard IB, Ivarsen A, Hjortdal J. Refractive correction and biomechanical strength following SMILE with a 110- or 160-mum cap thickness, evaluated ex vivo by inflation test. *Invest Ophthalmol Vis Sci*. 2018;59:1836–1843.
22. Güell JL, Verdaguer P, Mateu-Figueras G, et al. SMILE procedures with four different cap thicknesses for the correction of myopia and myopic astigmatism. *J Refract Surg*. 2015;31:580–585.
23. Qin B, Li M, Chen X, Sekundo W, Zhou X. Early visual outcomes and optical quality after femtosecond laser small-incision lenticule extraction for myopia and myopic astigmatism correction of over -10 dioptres. *Acta Ophthalmol*. 2018;96:e341–e346.
24. Ganesh S, Brar S. Femtosecond intrastromal lenticular implantation combined with accelerated collagen cross-linking for the treatment of keratoconus—initial clinical result in 6 eyes. *Cornea*. 2015;34:1331–1339.
25. Sun Y, Zhang T, Zhou Y, et al. Reversible femtosecond laser-assisted endokeratophakia using cryopreserved allogeneic corneal lenticule. *J Refract Surg*. 2016;32:569–576.
26. He M, Jin H, He H, et al. Femtosecond laser-assisted small incision endokeratophakia using a xenogeneic lenticule in rhesus monkeys. *Cornea*. 2018;37:354–361.
27. Liu YC, Teo EPW, Ang HP, et al. Biological corneal inlay for presbyopia derived from small incision lenticule extraction (SMILE). *Sci Rep*. 2018;8:1831.
28. Riau AK, Angunawela RI, Chaurasia SS, Lee WS, Tan DT, Mehta JS. Reversible femtosecond laser-assisted myopia correction: a non-human primate study of lenticule re-implantation after refractive lenticule extraction. *PLoS One*. 2013;8:e67058.
29. Zhao J, Zhao F, Huang J, Xu H, Chen Y, Zhou X. Two-year outcome of a patient treated with phototherapeutic keratectomy and autologous SMILE lenticule transplantation for flap-related complications following LASIK. *J Refract Surg*. 2018;34:281–285.
30. Mastropasqua L, Nubile M, Salgari N, Mastropasqua R. Femtosecond laser-assisted stromal lenticule addition keratoplasty for the treatment of advanced keratoconus: a preliminary study. *J Refract Surg*. 2018;34:36–44.
31. Ganesh S, Brar S, Rao PA. Cryopreservation of extracted corneal lenticules after small incision lenticule extraction for potential use in human subjects. *Cornea*. 2014;33:1355–1362.
32. Liu Y-C, Rosman M, Mehta JS. Enhancement after small-incision lenticule extraction. *Ophthalmology*. 2017;124:813–821.
33. Damgaard IB, Riau AK, Liu YC, Tey ML, Yam GH, Mehta JS. Reshaping and customization of SMILE-derived biological lenticules for intrastromal implantation. *Invest Ophthalmol Vis Sci*. 2018;59:2555–2563.
34. Liu YC, Williams GP, George BL, et al. Corneal lenticule storage before reimplantation. *Mol Vis*. 2017;23:753–764.
35. Mohamed-Noriega K, Toh KP, Poh R, et al. Cornea lenticule viability and structural integrity after refractive lenticule extraction (ReLEx) and cryopreservation. *Mol Vis*. 2011;17:3437–3449.
36. Yam GH, Yusoff NZ, Goh TW, et al. Decellularization of human stromal refractive lenticules for corneal tissue engineering. *Sci Rep*. 2016;6:26339.
37. Downie LE, Naranjo Golborne C, Chen M, et al. Recovery of the sub-basal nerve plexus and superficial nerve terminals after corneal epithelial injury in mice. *Exp Eye Res*. 2018;171:92–100.
38. Gatinel D, Hoang-Xuan T, Azar DT. Volume estimation of excimer laser tissue ablation for correction of spherical myopia and hyperopia. *Invest Ophthalmol Vis Sci*. 2002;43:1445–1449.
39. Vestergaard AH, Gronbech KT, Grauslund J, Ivarsen AR, Hjortdal JO. Subbasal nerve morphology, corneal sensation, and tear film evaluation after refractive femtosecond laser lenticule extraction. *Graef's Arch Clin Exp Ophthalmol*. 2013;251:2591–2600.
40. Cruzat A, Qazi Y, Hamrah P. In vivo confocal microscopy of corneal nerves in health and disease. *Ocul Surf*. 2017;15:15–47.
41. Bozkurt A, Lassner F, O'Dey D, et al. The role of micro-structured and interconnected pore channels in a collagen-based nerve guide on axonal regeneration in peripheral nerves. *Biomaterials*. 2012;33:1363–1375.
42. Carr MJ, Johnston AP. Schwann cells as drivers of tissue repair and regeneration. *Curr Opin Neurobiol*. 2017;47:52–57.
43. Kohama I, Lankford KL, Preiningerova J, White FA, Vollmer TL, Kocsis JD. Transplantation of cryopreserved adult human Schwann cells enhances axonal conduction in demyelinated spinal cord. *J Neurosci*. 2001;21:944–950.
44. Zhu Z, Qiao L, Zhao Y, Zhang S. Optimal freezing and thawing for the survival of peripheral nerves in severed rabbit limbs. *Int J Clin Exp Pathol*. 2014;7:7801–7805.
45. Darwish T, Brahma A, Efron N, O'Donnell C. Subbasal nerve regeneration after penetrating keratoplasty. *Cornea*. 2007;26:935–940.
46. Tervo T, Vannas A, Tervo K, Holden BA. Histochemical evidence of limited reinnervation of human corneal grafts. *Acta Ophthalmol*. 1985;63:207–214.

Investigative Ophthalmology & Visual Science